



HAL
open science

Evidence for Amorphous Sulfates as the Main Carrier of Soil Hydration in Gale Crater, Mars

Gaël David, Erwin Dehouck, P.-y. Meslin, W. Rapin, A. Cousin, O. Forni, O. Gasnault, J. Lasue, N. Mangold, P. Beck, et al.

► **To cite this version:**

Gaël David, Erwin Dehouck, P.-y. Meslin, W. Rapin, A. Cousin, et al.. Evidence for Amorphous Sulfates as the Main Carrier of Soil Hydration in Gale Crater, Mars. *Geophysical Research Letters*, 2022, 49 (21), pp.e2022GL098755. 10.1029/2022GL098755 . insu-03853102

HAL Id: insu-03853102

<https://insu.hal.science/insu-03853102>

Submitted on 15 Nov 2022

HAL is a multi-disciplinary open access archive for the deposit and dissemination of scientific research documents, whether they are published or not. The documents may come from teaching and research institutions in France or abroad, or from public or private research centers.

L'archive ouverte pluridisciplinaire **HAL**, est destinée au dépôt et à la diffusion de documents scientifiques de niveau recherche, publiés ou non, émanant des établissements d'enseignement et de recherche français ou étrangers, des laboratoires publics ou privés.



Distributed under a Creative Commons Attribution - NonCommercial - NoDerivatives 4.0 International License

Evidence for amorphous sulfates as the main carrier of soil hydration in Gale crater, Mars

David, G.¹, Dehouck, E.², Meslin, P.-Y.¹, Rapin, W.¹, Cousin, A.¹, Forni, O.¹, Gasnault, O.¹, Lasue, J.¹, Mangold, N.³, Beck, P.⁴, Maurice, S.¹, Wiens, R. C.^{5,6}, Berger, G.¹, Fabre, S.¹, Pinet, P.¹, Clark, B. C.⁷, Smith, J. R.⁸, Lanza, N. L.⁵

¹Institut de Recherche en Astrophysique et Planétologie, Université de Toulouse, CNRS, CNES, Toulouse, France

²Univ Lyon, UCBL, ENSL, UJM, CNRS, LGL-TPE, F-69622, Villeurbanne, France

³Laboratoire de Planétologie et Géodynamique, Nantes, CNRS UMR6112, Université de Nantes,

Université d'Angers, 44322 Nantes, France

⁴Univ Grenoble Alpes, CNRS, Institut de Planétologie et Astrophysique de Grenoble (IPAG), UMR 5274, Grenoble F-38041, France

⁵Los Alamos National Laboratory, Los Alamos, New Mexico, USA

⁶Earth, Atmospheric, and Planetary Sciences, Purdue University, West Lafayette, Indiana, USA

⁷Space Science Institute, Boulder, Colorado, USA

⁸Department of Geosciences, SUNY Stony Brook, Stony Brook, NY 11794, USA

Key Points:

- The amorphous component of Gale crater soils contains hydrated sulfates
- The eolian dust deposits are not the carrier of the identified hydrated sulfates
- Water-limited acidic conditions may have led to the formation of these phases

Corresponding author: David Gael, gdauid@irap.omp.eu

Abstract

Understanding the genesis of martian soils is important to constrain the hydrogeologic history of the planet. Soils have the potential to record paleoenvironmental conditions, through the nature of secondary minerals formed during weathering. *In situ* X-ray diffraction analyses in Gale crater have revealed that about one-third of each soil sample is composed of amorphous materials containing hydrated phases. Here, we use the geochemical data from the ChemCam instrument to investigate the nature and origin of the hydrated amorphous phases. We report for the first time with ChemCam clues for the presence of sulfates within the amorphous component of soils. We show that sulfates are the main carrier of the soil hydration and possibly explain the nature of hydrogen and sulfur measured from orbit. These sulfates and the apparent lack of significant Al-bearing weathering products are consistent with a model of soil formation including weathering of olivine in water-limited acidic conditions.

Plain Language Summary

The study of martian soils is of considerable interest as the nature of the mineral phases they contain, formed by the action of water for some of them, can give information on the past environments of the planet. Mineralogical analyses in Gale crater have shown that about one-third of soils are composed of poorly crystalline materials whose nature remains unclear, and that soil hydration could be associated with these phases. Here, we use the chemical analyses from the ChemCam instrument to investigate the composition of the hydrogen-bearing products, and we report for the first time the presence of sulfates in soils with this instrument. We demonstrate that sulfates are the main contributor to the water content of soils and are probably the source of the hydrogen and sulfur measured from orbit. The presence of sulfates and the lack of significant other secondary materials, especially enriched in aluminum, suggest that soils have probably undergone an acidic aqueous alteration with a low quantity of water, favoring the dissolution of olivine as the precursor to sulfates.

1 Introduction : the soils of Gale Crater

The chemical and mineralogical characterization of weathering products present in martian soils can reveal past aqueous processes that occurred on the planet. The term “soil” in the martian context refers to all loose, non-consolidated material, distinguishable from igneous or highly cohesive sedimentary rocks, and does not imply the presence or absence of organic matter or living organisms (e.g., Meslin et al. (2013); Certini et al. (2020)). Unlike regolith, which makes reference to unconsolidated mineral material with no implication on the nature of the mechanisms involved in pedogenesis, soil formation is the result of many processes that include physical and chemical alteration of rock precursors by wind action, impact and aqueous alteration (e.g., McSween et al. (2010); Certini et al. (2020)). Soils represent the accumulation of sediments from large volumes of crustal exposure, and aggregates derived from local, regional, and possibly global sources due to wind transport and mixing (e.g., McSween and Keil (2000); Yen et al. (2005); Newson et al. (2007); McSween et al. (2010)). They can record aqueous alteration processes during pedogenesis due to their fine size and large reactive surfaces compared to rocks. Therefore, determining the nature of the main constituents of soils can bring insights into the local, regional or even global aqueous history of Mars.

The Mars Science Laboratory (MSL) rover Curiosity landed in the 155 km diameter Gale crater, formed ~ 3.6 Gy in the Late Noachian/Early Hesperian (Le Deit et al., 2013). The first soil analyzed with the entire payload of the rover was the inactive eolian bedform of Rocknest on Sols 55-100 (Figure 1). This sand shadow deposit is still the best characterized martian soil to date, excluding the observation campaigns dedicated to the active sand dunes of Bagnold (Bridges & Ehlmann, 2017). From close-up

72 images (e.g., Figures 1.d, S1 and S2), Rocknest soils are composed of micrometer to milli-
73 meter-sized grains of varying colors, mixed with smaller dust particles easily transported
74 by the wind. Measurements by the Alpha Particle X-ray Spectrometer (APXS) instru-
75 ment show a bulk chemical composition overall similar to basaltic soils previously an-
76 alyzed *in situ* at Gusev crater and Meridiani Planum. This has been interpreted as the
77 possibility that martian soils could be homogeneous on a large scale (Yen et al., 2005;
78 Blake et al., 2013). However, substantial chemical differences have been observed in soils
79 from different martian regions by orbital data, which argues against complete mixing at
80 a global scale (Newsom et al., 2007). Within Gale crater itself, differences have been ob-
81 served between the Rocknest soils and the active dunes of Bagnold, which illustrates the
82 role of local contributions to soils composition (O’Connell-Cooper et al., 2017). Anal-
83 yses with the Laser-Induced Breakdown Spectroscopy (LIBS) instrument ChemCam iden-
84 tified two main components in the Rocknest soils: a coarse-grained anhydrous felsic com-
85 ponent, and a fine-grained hydrogen-rich mafic one that is very homogeneous all along
86 the rover traverse (Meslin et al., 2013; Cousin et al., 2015, 2017). X-ray diffraction (XRD)
87 analyses with CheMin show that the mineralogy of the Rocknest sieved sample (<150
88 μm) is mainly composed of igneous basaltic phases, and despite being nearly ubiquitous
89 in the sedimentary rocks of Gale, no clay mineral was detected in the soils. Only a few
90 secondary minerals have been identified such as anhydrite, magnetite (potentially igneous),
91 and hematite in minor abundances (Bish et al., 2013; Achilles et al., 2017). However, 35 ± 15
92 wt.% of the Rocknest sample correspond to X-ray amorphous phases (i.e., poorly crys-
93 talline or nanophase materials), whose nature remains unclear. Martian soils have long
94 been suspected to contain an amorphous component based on orbital and *in situ* anal-
95 yses (e.g., Evans and Adams (1979); Singer (1985); Morris et al. (2000); Squyres et al.
96 (2008)).

97 Mass balance calculations using APXS bulk chemistry of the Portage soil target
98 (containing both fine and coarse particles) and CheMin mineralogy at Rocknest suggest
99 that the amorphous component is enriched in FeO_T , Na_2O , K_2O , TiO_2 , SO_3 , P_2O_5 , Cr_2O_3 ,
100 MnO , Cl and depleted in SiO_2 , Al_2O_3 , CaO , MgO relative to the crystalline counterpart
101 (Blake et al., 2013; Achilles et al., 2017). Importantly, as CheMin did not detect any hy-
102 drated mineral, the ~ 2 wt.% H_2O quantified in the sieved fraction by the SAM instru-
103 ment (Leshin et al., 2013; Sutter et al., 2017), and the H signal mostly recorded in the
104 fine-grained component by ChemCam (Meslin et al., 2013; Cousin et al., 2015) must be
105 mostly associated with the amorphous component, although hydrated crystalline phases
106 could be present below the CheMin’s detection limit (~ 1 wt.%; Rampe et al. (2020)),
107 and some H could be contained as impurities in the phases detected by CheMin. The
108 estimated chemical composition of the amorphous component with the mass balance cal-
109 culations cannot be explained with primary basaltic glass only, and necessarily involves
110 a mixture of several phases (Bish et al., 2013; Dehouck et al., 2014; Achilles et al., 2017)
111 that could include both primary materials (volcanic and/or impact glass) and secondary
112 products (e.g., poorly crystalline silicates, nanophase iron oxides, amorphous sulfates).
113 Determining precisely the chemical composition of the major phases constituting the amor-
114 phous component is necessary to understand its nature and constrain its origin. Further-
115 more, amorphous phases could represent the main carriers of the ubiquitous hydrogen
116 measured from orbit by Mars Odyssey at low and mid-latitudes (Boynton et al., 2007;
117 Newsom et al., 2007; Karunatillake et al., 2014).

118 In this paper, we use the geochemical data acquired with the ChemCam instrument
119 in the soils of Bradbury rise, Rocknest and Yellowknife Bay area (Figure 1.a) to char-
120 acterize the chemical composition of the hydrated phases thought to be associated with
121 the amorphous component. Due to its submillimeter sampling area (i.e., 350-550 μm di-
122 ameter) and its sensitivity to hydrogen and other volatile species, ChemCam is well suited
123 to study alteration products. It provides a new methodology to constrain their chem-
124 ical compositions and to give insight into the weathering history of the planet.

Figure 1. a) HiRISE mosaic showing the Curiosity’s traverse from the landing site at Sol 0 up to Sol 194. The Bradbury, Rocknest and Yellowknife Bay area are displayed, as well as the localization and the name (in yellow) of the 25 soils analyzed by ChemCam used in this study (NASA/Caltech-JPL/Univ. of Arizona). b) Mastcam mosaic showing the Rocknest patch of soil on Sol 52, which is about 1.5 meters by 5 meters (NASA/Caltech-JPL/MSSS). c) Mast-Cam image of the scooped samples of Rocknest during Sol 93 (0093ML0005450000102912E01, NASA/Caltech-JPL/MSSS) d) Footprint of the Curiosity wheel in the Rocknest soils seen with the MastCam instrument on Sol 59 (0059MR0002680030103132E01, NASA/Caltech-JPL/MSSS). e) MAHLI image on Sol 95 of the sieved fraction ($<150 \mu\text{m}$) of the Rocknest soils on the titanium observation tray of the rover (0095MH0001310000101120C00, NASA/Caltech-JPL/MSSS).

2 Materials and Methods

2.1 The ChemCam LIBS instrument

The ChemCam instrument (Wiens et al., 2012; Maurice et al., 2012) is the first generation of LIBS instrument launched to Mars. It provides remote analyses of the major rock-forming elements as well as some minor and trace elements, at a sub-millimeter scale. A nanosecond pulsed laser (1067 nm) is focused on the sample with a telescope generating a plasma of excited ions, atoms, and molecules. As the plasma cools down, excited species release energy in the form of light that is collected by the telescope and analyzed by three spectrometers in the 240.1 - 342.2 nm (ultraviolet), 382.1 - 469.3 nm (violet), and 474.0 - 906.5 nm (visible and near-infrared) spectral ranges. For each ChemCam observation point, repeated laser shots are fired (typically with bursts of 30 shots), and each laser shot yields a LIBS spectrum. As detailed in Wiens et al. (2013) and Clegg et al. (2017), ChemCam data are processed by removing the nonlaser reflectance spectrum (“dark spectrum”), denoised, corrected for the continuum emission, and finally wavelength calibrated and corrected for the instrument response.

2.2 Quantitative and qualitative analyses of ChemCam data

From ChemCam spectra, major oxide (i.e., SiO_2 , TiO_2 , Al_2O_3 , MgO , CaO , Na_2O , K_2O) quantification is made using a large library of spectra acquired on geological standards (>400 samples) and two multivariate analysis algorithms: a partial least squares (PLS, Clegg et al. (2017)), and an independent component analysis (ICA, Forni et al. (2013)). For iron quantification, we used here a dedicated calibration method described in David et al. (2020), more appropriate to highlight the presence of Fe-rich mineral phases in the ChemCam shot-to-shot dataset. The major composition is not normalized to 100 wt.% to take into account volatile concentrations including H and S contents.

Indeed, unlike major elements, hydrogen is not yet quantified in granular media, and we used instead the independent component analysis (Forni et al., 2013) to investigate the variation of H signal in ChemCam data (expressed in the form of ICA scores).

Sulfur abundance is estimated in ChemCam data from the 564 nm emission peak area, normalized to the oxygen peak area at 778 nm, following the method defined in Rapin et al. (2019). This approach was successfully used to detect the presence of Ca- and Mg-sulfates in the matrix of the sedimentary rocks of the Murray formation.

2.3 Data selection

In this study, we selected the soil targets analyzed by ChemCam from Sol 19 to 194 localized in the Bradbury, Rocknest and Yellowknife Bay area (Figure 1.a). The ChemCam Remote Micro-Imager is used to consider only observation points located on gran-

ular soils. LIBS spectra with a noise level too high for sulfur peak analyses (i.e., with total spectral intensity lower than 1.6×10^{14} photons) are removed from our dataset. In the end, the ChemCam dataset used in this study corresponds to 25 soil targets. ChemCam analyses are rasters of several observation points, and a burst of laser shots is performed on each of these points. As a result, our 25 soil targets translate into 165 different LIBS observation points and 4790 single-shot LIBS spectra.

Finally, we distinguished in our data LIBS shots that probed the dust from the rest of the soil. Indeed, the inactive Rocknest soils are covered with a thin layer of eolian dust deposits, and its composition can be estimated considering the first LIBS shot of each ChemCam laser burst as shown by Lasue et al. (2018).

3 Results

3.1 Chemical characterization of soils with ChemCam

When plotted in diagrams showing major oxides constituting soils as a function of the ICA H scores, the shot-to-shot scatter shows several mixing lines with at least three end-members (Figure 2.a, c-i). Two of them trend towards low H contents, indicating that the corresponding LIBS shots mainly probed anhydrous mineral mixtures, whereas the third end-member is hydrated. Similar data trends are observed in soils located in the Rocknest area and soils located in the Bradbury rise and Yellowknife Bay (cf. Figure S3), indicating similar mineral mixtures between these sites.

In figure 2, the scatter of the ChemCam shot-to-shot data shows several trends toward anhydrous mineral phases. This is in agreement with the composition of the main igneous mineral phases identified by CheMin (shown by diamonds in Figure 2), except for K_2O and TiO_2 . We first show that ChemCam successfully discriminated the mafic and felsic components in soils, and that it is able to constrain the chemical composition of individual phases (or a group of phases with similar composition). LIBS spectra have been grouped into different classes based on their level of hydration and Al_2O_3 abundances (cf. S5). Groups 1 and 2 correspond to the two anhydrous end-members (ICA H score < 0.031) with respectively low and high Al_2O_3 contents (i.e., < 10.6 wt.% and > 17.8 wt.%). While LIBS shots from group 1 are depleted in Al_2O_3 relative to group 2 by definition, they are relatively rich in MgO , FeO_T , and TiO_2 (Figure 3.a, b, i) with average values of 8.0, 18, and 1 wt.%; and thus mainly reflect the olivine, augite, and pigeonite minerals identified by CheMin (respectively ~ 17 , ~ 14 , and ~ 7 wt.% in the Rocknest soils; Bish et al. (2013); Achilles et al. (2017)). On the other hand, group 2 is rich in Al_2O_3 relative to group 1, and also enriched on average in SiO_2 (54.4 wt.%), CaO (8.9 wt.%), and Na_2O (5.9 wt.%) as seen in Figure 3.d, e, g. Such chemistry is consistent with plagioclase minerals, which is the most abundant crystalline phase detected by CheMin (~ 24 wt.%, Bish et al. (2013); Achilles et al. (2017)). The sulfur signal from the 564 nm peak area is low and roughly equal for groups 1 and 2 (Figure 3.c), which is expected for such igneous minerals. K_2O appears defined to be weakly discriminating between the mafic and felsic populations (Figure 3.h), in agreement with the fact that K-feldspar was not identified in the $< 150 \mu m$ Rocknest soils (Bish et al., 2013; Achilles et al., 2017) and should be present only in minor abundance if any. K-rich and Ti-rich spectra observed in figure 2.h and 2.i should be then mostly associated with anhydrous K-bearing and Ti-bearing phases with amorphous natures or/and linked to coarser minerals than those analyzed by CheMin or/and in abundance below CheMin's detection limit.

The hydrogen-rich end-member observed in Figure 2 should correspond to the soil fraction associated with the hydrated amorphous component. The increase in hydration observed in some spectra is significant and reaches more than three times the average hydration value observed in bulk soils. From our estimate of water content, based on the average ICA score in soils and H SAM analyses (Figure 2.a, text S1), this would correspond to targets containing more than ~ 6 wt.% H_2O . Interestingly, a correlation is observed between H and S (Figure 2.b). This indicates that soil hydration is principally

Figure 2. Single-laser-shot compositions plotted against ICA hydrogen scores for the 25 ChemCam soil targets acquired in the Bradbury rise, Rocknest and Yellowknife Bay area. The first LIBS shot of each ChemCam laser burst (orange squares) reflects the chemical composition of the eolian dust. The chemical composition of mineral phases identified by CheMin (*) in the <150 μm fraction of Rocknest soils and the composition of the amorphous component (***) are also shown (from Achilles et al. (2017)). The red lines connecting the main igneous minerals observed by CheMin to the average abundances measured with ChemCam in the bulk soils express expected trends in the ChemCam shot-to-shot scatter. See text S1 for details on the estimates of H_2O and SO_3 abundances.

212 carried by S-bearing phases such as sulfates rather than poorly crystalline silicates or
 213 nanophase iron hydroxides. In addition, hydrogen-rich spectra show MgO , FeO_T and CaO
 214 abundances around the average of the bulk soils, while SiO_2 , TiO_2 , Al_2O_3 , Na_2O , and
 215 K_2O contents are among the lowest recorded.

216 This is also observed when comparing the distribution of major elements between
 217 the different groups of LIBS spectra representing different chemical compositions (Fig-
 218 ure 3): the groups 1 and 2 (of relatively mafic and felsic compositions respectively, and
 219 will therefore be referred to as "mafic" and "felsic" in the rest of the paper, for concise-
 220 ness) and the hydrated component (group 3, ICA H score >0.056). From figure 3, the
 221 hydrated group appears to have a composition mostly similar to the mafic-type, but with
 222 high S and H contents. On average, the MgO abundances are similar between the hy-
 223 drated (8.1 ± 1.9 wt.%) and the mafic (8 ± 2.5 wt.%) groups, and FeO_T and SiO_2 abun-
 224 dances are only slightly higher in the mafic component (respectively $15.5 \pm 2.9 /$
 225 17.6 ± 3.9 wt.% and $41.6 \pm 3.5 / 43.4 \pm 3.9$ wt.%).

226 Due to the overall similar composition between the hydrogen and mafic groups, no
 227 linear correlation is observed between H and other major elements (except S). However,
 228 the similar MgO average values in the S- and H-rich group and the mafic one shows the
 229 presence of hydrated Mg-S rich phases such as Mg-sulfates within the XRD amorphous
 230 component of soils. Although a strong increase of H and S abundances is observed in some
 231 LIBS spectra (up to more than ~ 6 wt.% H_2O and between ~ 10.6 - 15.9 wt.% SO_3 ; cf. Fig-
 232 ures 2), the Mg contents remain overall constant in these points. Consequently, the H-
 233 and S-rich phases must be associated, at least partially, with Mg cations because oth-
 234 erwise some dilution effects should occur and a drop of the Mg content should be observed.
 235 The same reasoning holds for Fe and Ca. In the hydrated end-member, the high S sig-
 236 nal and FeO_T content compared to the felsic component could suggest that Fe-bearing
 237 sulfates are also present. However, intimate mixtures of Mg-sulfates with ferric oxyhy-
 238 droxides (e.g., ferrihydrite) cannot be totally ruled out by LIBS analyses alone. Indeed,
 239 due to the nanoparticulate nature of the latter minerals, their chemical composition can
 240 be diluted with other major phases, making their detection difficult (e.g., David et al.
 241 (2020)). The CaO abundance of the H-rich group is lower than the felsic-type group and
 242 rather consistent with the mafic end-member. Given the lack of decrease in CaO con-
 243 tent associated with the volatile-rich point, the presence of Ca-sulfates is also likely. Oth-
 244 erwise, the low Al_2O_3 abundances associated with H-rich spectra suggest that allophane
 245 (poorly crystalline phyllosilicate), which is particularly expected during the alteration
 246 of volcanic glass (Chadwick et al., 2003), is unlikely to be a main component in soils, as
 247 also supported by the low Al_2O_3 content estimated with the APXS-CheMin mass bal-
 248 ance calculations (~ 5.45 wt.%; Bish et al. (2013); Dehouck et al. (2014); Achilles et al.
 249 (2017)). The lack of Al_2O_3 and SiO_2 enrichment associated with S-rich spectra (Figures
 250 2 and S4) also suggests that the sorption of sulfate ions onto Al-phyllosilicates or their
 251 precursors is not the prevailing mechanism to host this element in soils.

ChemCam laser shots reflecting the dust composition are shown in figure 2 (orange squares). The dust fraction of soils contains a significant hydrogen content, consistent with previous ChemCam studies (Meslin et al., 2013; Lasue et al., 2018). However, the hydrated sulfates identified here are not hosted by the eolian dust as seen from the scatter of the ICA H scores. Indeed, we observe that there are LIBS spectra from the bulk soils ($\sim 26.7\%$ of total number of spectra) that show a higher hydration than the average value of the dust plus uncertainty (i.e., 0.045 ± 0.009). This implies that the dust does not correspond to the hydrated end-member, and that discrete particles of hydrated sulfates coarser than the aeolian dust are present within the soil material itself, or that sulfates are present as rinds or coatings around igneous grains. Nevertheless, it is a possibility that the dust is composed of the same mafic, felsic, and hydrated minerals identified, but with smaller grain sizes. We are however unable to address this question, because at such small grain size the LIBS technique does not provide a composition for individual grains, instead averaging the composition of a number of grains together, as observed in laboratory experiments (David et al., 2021).

Figure 3. Box plots showing the distribution of major elements (MgO, FeO_T, S, CaO, SiO₂, Al₂O₃, Na₂O, K₂O and TiO₂) in 3 groups of LIBS spectra. Groups 1 (red) and 2 (green) correspond to anhydrous end-members (ICA H score < 0.031) with respectively low and high Al₂O₃ abundances (i.e., lower than 10.6 wt.% and higher than 17.8 wt.%), whereas groups 3 (blue) correspond to end-members with high hydrogen contents (ICA H score > 0.056).

4 Discussion

4.1 Discussion on the presence of hydrated sulfates

The detection of sulfates with ChemCam is compatible with the evolved gas analyses (EGA) performed by the SAM instrument onboard Curiosity, which recorded SO₂ releases during pyrolysis at temperatures consistent with several candidates including crystalline or amorphous Mg- and Fe-sulfates, as well as adsorbed sulfate forms (Leshin et al., 2013; Sutter et al., 2017). The temperature of water release measured by SAM is also consistent with structural H₂O or OH from sulfates, although several other phases are possible (Archer et al., 2014). Unfortunately, all Ca-sulfates decompose at temperatures beyond the SAM range and thus cannot be detected by the instrument (McAdam et al., 2014). The APXS-CheMin mass balance calculations (Blake et al., 2013; Achilles et al., 2017) indicate a sulfur budget for the amorphous component (14.04 wt.% SO₃) that is in excess to contain only Mg-sulfates given its magnesium budget (4.05 wt.% MgO) and Fe-sulfates and/or Ca-sulfates must be also present.

Mg-, Fe-, and Ca-sulfates are weathering constituents of other martian soils studied *in situ* in the Chryse and Utopia Planitia, in the high latitudes of Vastitas Borealis, and in Ares Vallis and Gusev crater, as suggested by the Viking and Phoenix landers (Clark, 1993; Kounaves et al., 2010), and by the Pathfinder and Spirit rovers (Foley et al., 2003; Wang et al., 2006; Yen et al., 2008; Lane et al., 2008). While it has been demonstrated that soils at Gale have chemical compositions overall similar to other soils studied in different locations of the planet (e.g., Yen et al. (2005); Blake et al. (2013)), here we establish that they also share some mineralogical properties. This observation is in line with the idea that these soils could have a common history, due to large scale soil homogenization by wind transport followed by mixing, and/or due to similar source materials and alteration processes. In the latter case, a regionally localized provenance of sulfates and other soil components is still allowed. In Gale's soils, the nearly identical sulfur abundances with the soils of Gusev and Meridiani (Blake et al., 2013) suggest that

the sulfates found in Rocknest do not need to originate from the mechanical erosion of the uppermost sulfate-rich strata of Aeolis Mons.

In situ analyses showing that sulfates are the main carrier of soil hydration in Gale are also consistent with orbital observations at a broad scale. In the southern highlands, the H₂O signatures from orbit are correlated with sulfur concentrations (Karunatillake et al., 2014; Hood et al., 2019), supporting our finding and the central role of hydrated sulfates in the water distribution of martian soils.

4.2 Possible formation process of the amorphous sulfates

The presence of Mg-sulfates (and likely Fe-sulfates) combined with the apparent lack of significant Al-bearing secondary phases hints at some specific conditions during aqueous alteration and formation of soils. Mg-sulfates are expected to be among the predominant minerals formed along with Fe-sulfates, poorly crystalline Fe-oxides, and amorphous silica during chemical weathering of basaltic materials at low water activity, low-pH, and sulfuric acid-rich environment (Banin et al., 1997; Golden et al., 2005; Tosca et al., 2004, 2005; Hurowitz et al., 2006; Hurowitz & McLennan, 2007). In an acidic environment, a low water-to-rock ratio promotes the stoichiometric alteration of olivine relative to other igneous minerals and basaltic glasses, which have lower dissolution rates (Hurowitz & McLennan, 2007). Slow weathering during cold and dry conditions on Mars, through interactions of basaltic materials with volcanic aerosols, frost, or thin films of transient liquid water along grain boundaries loaded with volcanically derived volatile species are sustainable scenarios to explain our observations, as modeled by Treguier et al. (2008) and Berger et al. (2009). In these conditions, the chemical budget for secondary mineralogy subsequent to olivine dissolution is dominated by Mg, Fe, and Si, and the formation of significant Al-bearing alteration phases (Al-sulfates, Al-hydroxides, and phyllosilicates) is inhibited as Al-rich primary silicates and Al-bearing glasses are mostly unaltered. In such scenario, Ca-sulfates are not expected to be produced in high abundance and those in soils could be formed by a different process.

Several mechanisms can cause these sulfates to become then XRD amorphous. The mineralogy and hydration state of sulfates, and in particular for magnesium-bearing species, are highly dependent on relative humidity and temperature. First, it is possible that the nature of sulfates changed during the first hours of analysis inside the warm and therefore low relative humidity environment of CheMin, and that sulfates were originally crystalline before the samples were collected (Vaniman et al., 2018). Alternatively, the sulfate amorphization process could also occur during their formation (e.g., from rapid evaporation or freezing of saline solutions (Vaniman & Chipera, 2006; Morris et al., 2015)), or during diagenesis after partial dehydration of crystalline phases (Vaniman et al., 2004; Chipera & Vaniman, 2007). At their time of formation, sulfates with higher hydration state may have been present in soils, and dehydrated during environmental changes causing their amorphization, possibly reflecting diurnal variations or changes in orbital parameters of the planet.

5 Conclusions

The chemical composition of the weathering products constituting the soils of the martian surface provides important clues about the aqueous environments in which they formed. By investigating the hydrogen signal recorded by the ChemCam instrument on-board Curiosity in the soils of the Bradbury rise, Rocknest and Yellowknife Bay area, we have identified the main hydrogen-bearing products, and bring new constraints into our comprehension of martian pedogenesis. We make the first direct chemical association between H and S, revealing the presence of hydrated sulfates in the soils of Gale crater. These sulfates, carriers of the soil hydration, are amorphous since CheMin did not detect them, or any hydrated crystalline mineral. Due to the relatively high Mg, Fe and

344 Ca contents associated with the sulfur-rich spectra, mixture of Mg-, Fe-, and Ca-sulfates
345 could be present, which is consistent with results from other instruments onboard Cu-
346 riosity such as SAM or the APXS-CheMin mass balance calculations (Blake et al., 2013;
347 Achilles et al., 2017; Sutter et al., 2017).

348 In this study, we establish that the soils of Gale contain similar sulfates than ob-
349 served *in situ* in other locations of the planet, reinforcing the idea that soils on Mars may
350 have a common history. Given the predominance of hydrated sulfates among alteration
351 products in the soils of Gale, and the lack of Al-bearing secondary mineral like phyllosil-
352 icates, we assumed that soils have undergone an overall low grade of chemical alteration
353 and that sulfate formation likely occurred at low water activity under acidic conditions,
354 promoting dissolution of labile minerals such as olivine. The amorphization process of
355 sulfates could occur either at their time of formation or later during diagenesis, poten-
356 tially induced by environmental changes on the martian surface.

357 Acknowledgments

358 We gratefully acknowledge the Mars Science Laboratory scientific and engineer-
359 ing teams for enabling the collection of the datasets used in this study. This research was
360 carried out with financial support from NASA's Mars Exploration Program in the US
361 and in France with the Centre National d'Etudes Spatiales (CNES). We thank the MAHLI
362 and Mastcam teams at Malin Space Science Systems for processing the images used in
363 this paper.

364 Open research

365 Data Availability Statement

366 All ChemCam data used in this study are publicly available on the Planetary Data
367 System (<http://pds-geosciences.wustl.edu/missions/msl/chemcam.htm>). Complete list
368 of targets and chemical compositions can be found in the Zenodo open-source online repos-
369 itory (David et al., 2022).

370 **References**

- 371 Achilles, C., Downs, R. T., Ming, D., Rampe, E., Morris, R., Treiman, A., ... others
372 (2017). Mineralogy of an active eolian sediment from the Namib Dune, Gale
373 Crater, Mars. *Journal of Geophysical Research: Planets*, *122*(11), 2344–2361.
- 374 Archer, P. D., Franz, H. B., Sutter, B., Arevalo Jr, R. D., Coll, P., Eigenbrode,
375 J. L., ... others (2014). Abundances and implications of volatile-bearing
376 species from evolved gas analysis of the Rocknest aeolian deposit, Gale Crater,
377 Mars. *Journal of Geophysical Research: Planets*, *119*(1), 237–254.
- 378 Banin, A., Han, F., Kan, I., & Cicelsky, A. (1997). Acidic volatiles and the Mars
379 soil. *Journal of Geophysical Research: Planets*, *102*(E6), 13341–13356.
- 380 Berger, G., Toplis, M. J., Treguier, E., d’Uston, C., & Pinet, P. (2009). Evidence in
381 favor of small amounts of ephemeral and transient water during alteration at
382 Meridiani Planum, Mars. *American Mineralogist*, *94*(8-9), 1279–1282.
- 383 Bish, D. L., Blake, D., Vaniman, D., Chipera, S., Morris, R., Ming, D., ... others
384 (2013). X-ray diffraction results from Mars Science Laboratory: Mineralogy of
385 Rocknest at Gale Crater. *science*, *341*(6153), 1238932.
- 386 Blake, D. F., Morris, R. V., Kocurek, G., Morrison, S., Downs, R. T., Bish, D., ...
387 others (2013). Curiosity at Gale Crater, Mars: Characterization and analysis
388 of the Rocknest sand shadow. *Science*, *341*(6153), 1239505.
- 389 Boynton, W. V., Taylor, G., Evans, L. G., Reedy, R., Starr, R., Janes, D., ... others
390 (2007). Concentration of H, Si, Cl, K, Fe, and Th in the low-and mid-latitude
391 regions of Mars. *Journal of Geophysical Research: Planets*, *112*(E12).
- 392 Bridges, N., & Ehlmann, B. (2017). The Mars Science Laboratory (MSL) Bagnold
393 Dunes campaign, phase i: Overview and introduction to the special issue: Bag-
394 nold Dunes campaign overview. *Journal of Geophysical Research: Planets*,
395 *122*.
- 396 Cardoso, J.-F. (1997). Infomax and maximum likelihood for blind source separation.
397 *IEEE Signal processing letters*, *4*(4), 112–114.
- 398 Certini, G., Karunatillake, S., Zhao, Y.-Y. S., Meslin, P.-Y., Cousin, A., Hood,
399 D. R., & Scalenghe, R. (2020). Disambiguating the soils of mars. *Planetary*
400 *and Space Science*, 104922.
- 401 Chadwick, O. A., Gavenda, R. T., Kelly, E. F., Ziegler, K., Olson, C. G., Elliott,
402 W. C., & Hendricks, D. M. (2003). The impact of climate on the biogeochemi-
403 cal functioning of volcanic soils. *Chemical Geology*, *202*(3-4), 195–223.
- 404 Chipera, S. J., & Vaniman, D. T. (2007). Experimental stability of magnesium
405 sulfate hydrates that may be present on Mars. *Geochimica et Cosmochimica*
406 *Acta*, *71*(1), 241–250.
- 407 Clark, B. C. (1993). Geochemical components in martian soil. *Geochimica et Cos-*
408 *mochimica Acta*, *57*(19), 4575–4581.
- 409 Clegg, S. M., Wiens, R. C., Anderson, R., Forni, O., Frydenvang, J., Lasue, J., ...
410 others (2017). Recalibration of the Mars Science Laboratory ChemCam instru-
411 ment with an expanded geochemical database. *Spectrochimica Acta Part B:*
412 *Atomic Spectroscopy*, *129*, 64–85.
- 413 Cousin, A., Dehouck, E., Meslin, P.-Y., Forni, O., Williams, A. J., Stein, N., ...
414 others (2017). Geochemistry of the Bagnold Dune field as observed by Chem-
415 Cam and comparison with other aeolian deposits at Gale Crater. *Journal of*
416 *Geophysical Research: Planets*, *122*(10), 2144–2162.
- 417 Cousin, A., Meslin, P., Wiens, R., Rapin, W., Mangold, N., Fabre, C., ... others
418 (2015). Compositions of coarse and fine particles in martian soils at Gale: A
419 window into the production of soils. *Icarus*, *249*, 22–42.
- 420 David, G., Cousin, A., Forni, O., Meslin, P.-Y., Dehouck, E., Mangold, N., ... oth-
421 ers (2020). Analyses of high-iron sedimentary bedrock and diagenetic features
422 observed with ChemCam at vera rubin ridge, Gale Crater, Mars: calibra-
423 tion and characterization. *Journal of Geophysical Research: Planets*, *125*(8),
424 e2019JE006314.

- 425 David, G., Dehouck, E., Meslin, P.-Y., Rapin, W., Cousin, A., Forni, O., . . . Lanza,
426 N. L. (2022). Supplemental information data from: "Evidence for amorphous
427 sulfates as the main carrier of soil hydration in Gale crater, Mars".
428 doi: 10.5281/zenodo.7015277
- 429 David, G., Meslin, P.-Y., Dehouck, E., Gasnault, O., Cousin, A., Forni, O., . . . oth-
430 ers (2021). Laser-induced breakdown spectroscopy (LIBS) characterization
431 of granular soils: Implications for ChemCam analyses at Gale Crater, Mars.
432 *Icarus*, 114481.
- 433 Dehouck, E., McLennan, S. M., Meslin, P.-Y., & Cousin, A. (2014). Constraints on
434 abundance, composition, and nature of X-ray amorphous components of soils
435 and rocks at Gale Crater, Mars. *Journal of Geophysical Research: Planets*,
436 119(12), 2640–2657.
- 437 Evans, D. L., & Adams, J. B. (1979). Comparison of Viking lander multispectral
438 images and laboratory reflectance spectra of terrestrial samples. In *Lunar and*
439 *planetary science conference proceedings* (Vol. 10, pp. 1829–1834).
- 440 Foley, C. N., Economou, T., & Claylon, R. N. (2003). Final chemical results from
441 the Mars Pathfinder alpha proton X-ray spectrometer: Mars exploration rover
442 mission and landing sites. *Journal of geophysical research*, 108(E12), ROV37–
443 1.
- 444 Forni, O., Maurice, S., Gasnault, O., Wiens, R. C., Cousin, A., Clegg, S. M., . . .
445 Lasue, J. (2013). Independent component analysis classification of laser in-
446 duced breakdown spectroscopy spectra. *Spectrochimica Acta Part B: Atomic*
447 *Spectroscopy*, 86, 31–41.
- 448 Golden, D., Ming, D. W., Morris, R. V., & Mertzman, S. A. (2005). Laboratory-
449 simulated acid-sulfate weathering of basaltic materials: Implications for for-
450 mation of sulfates at Meridiani Planum and Gusev Crater, Mars. *Journal of*
451 *Geophysical Research: Planets*, 110(E12).
- 452 Hood, D., Karunatillake, S., Gasnault, O., Williams, A., Dutrow, B., Ojha, L., . . .
453 Fralick, C. (2019). Contrasting regional soil alteration across the topographic
454 dichotomy of Mars. *Geophysical Research Letters*, 46(23), 13668–13677.
- 455 Hurowitz, J. A., & McLennan, S. M. (2007). A 3.5 Ga record of water-limited, acidic
456 weathering conditions on Mars. *Earth and Planetary Science Letters*, 260(3-4),
457 432–443.
- 458 Hurowitz, J. A., McLennan, S. M., Tosca, N. J., Arvidson, R. E., Michalski, J. R.,
459 Ming, D. W., . . . Squyres, S. W. (2006). In situ and experimental evidence for
460 acidic weathering of rocks and soils on Mars. *Journal of Geophysical Research:*
461 *Planets*, 111(E2).
- 462 Karunatillake, S., Wray, J., Gasnault, O., McLennan, S., Rogers, A., Squyres, S., . . .
463 Olsen, N. (2014). Sulfates hydrating bulk soil in the martian low and middle
464 latitudes. *Geophysical Research Letters*, 41(22), 7987–7996.
- 465 Kounaves, S. P., Hecht, M. H., Kapit, J., Quinn, R. C., Catling, D. C., Clark, B. C.,
466 . . . others (2010). Soluble sulfate in the martian soil at the Phoenix landing
467 site. *Geophysical Research Letters*, 37(9).
- 468 Lane, M. D., Bishop, J. L., Darby Dyar, M., King, P. L., Parente, M., & Hyde,
469 B. C. (2008). Mineralogy of the Paso Robles soils on Mars. *American Mineral-*
470 *ogist*, 93(5-6), 728–739.
- 471 Lasue, J., Cousin, A., Meslin, P.-Y., Mangold, N., Wiens, R. C., Berger, G., . . . oth-
472 ers (2018). Martian eolian dust probed by ChemCam. *Geophysical Research*
473 *Letters*, 45(20), 10–968.
- 474 Le Deit, L., Hauber, E., Fueten, F., Pondrelli, M., Rossi, A. P., & Jaumann, R.
475 (2013). Sequence of infilling events in Gale Crater, Mars: Results from mor-
476 phology, stratigraphy, and mineralogy. *Journal of Geophysical Research:*
477 *Planets*, 118(12), 2439–2473.
- 478 Le Mouélic, S., Gasnault, O., Herkenhoff, K., Bridges, N., Langevin, Y., Mangold,
479 N., . . . others (2015). The ChemCam remote micro-imager at Gale Crater:

- 480 Review of the first year of operations on Mars. *Icarus*, *249*, 93–107.
- 481 Leshin, L., Mahaffy, P., Webster, C., Cabane, M., Coll, P., Conrad, P., . . . others
482 (2013). Volatile, isotope, and organic analysis of martian fines with the Mars
483 Curiosity rover. *Science*, *341*(6153), 1238937.
- 484 Maurice, S., Wiens, R., Saccoccio, M., Barraclough, B., Gasnault, O., Forni, O., . . .
485 others (2012). The ChemCam instrument suite on the Mars Science Labora-
486 tory (MSL) rover: Science objectives and Mast Unit description. *Space science*
487 *reviews*, *170*(1-4), 95–166.
- 488 McAdam, A. C., Franz, H. B., Sutter, B., Archer Jr, P. D., Freissinet, C., Eigen-
489 brode, J. L., . . . others (2014). Sulfur-bearing phases detected by evolved
490 gas analysis of the Rocknest aeolian deposit, Gale Crater, Mars. *Journal of*
491 *Geophysical Research: Planets*, *119*(2), 373–393.
- 492 McSween, H. Y., & Keil, K. (2000). Mixing relationships in the martian regolith
493 and the composition of globally homogeneous dust. *Geochimica et Cosmochim-*
494 *ica Acta*, *64*(12), 2155–2166.
- 495 McSween, H. Y., McGlynn, I. O., & Rogers, A. D. (2010). Determining the
496 modal mineralogy of martian soils. *Journal of Geophysical Research: Plan-*
497 *ets*, *115*(E7).
- 498 Meslin, P.-Y., Gasnault, O., Forni, O., Schröder, S., Cousin, A., Berger, G., . . . oth-
499 ers (2013). Soil diversity and hydration as observed by ChemCam at Gale
500 Crater, Mars. *Science*, *341*(6153), 1238670.
- 501 Morris, R. V., Golden, D., Bell, J. F., Shelfer, T. D., Scheinost, A. C., Hinman,
502 N. W., . . . others (2000). Mineralogy, composition, and alteration of Mars
503 Pathfinder rocks and soils: Evidence from multispectral, elemental, and mag-
504 netic data on terrestrial analogue, SNC meteorite, and Pathfinder samples.
505 *Journal of Geophysical Research: Planets*, *105*(E1), 1757–1817.
- 506 Morris, R. V., Rampe, E., Graff, T., Archer Jr, P., Le, L., Ming, D., & Sutter, B.
507 (2015). Transmission X-ray diffraction (XRD) patterns relevant to the MSL
508 CheMin amorphous component: Sulfates and silicates. In *Lunar and planetary*
509 *science conference* (Vol. 46).
- 510 Newsom, H. E., Crumpler, L. S., Reedy, R. C., Petersen, M. T., Newsom, G. C.,
511 Evans, L. G., . . . others (2007). Geochemistry of martian soil and bedrock in
512 mantled and less mantled terrains with gamma ray data from Mars odyssey.
513 *Journal of Geophysical Research: Planets*, *112*(E3).
- 514 O’Connell-Cooper, C., Spray, J., Thompson, L., Gellert, R., Berger, J., Boyd, N., . . .
515 VanBommel, S. (2017). APXS-derived chemistry of the Bagnold Dune sands:
516 Comparisons with Gale Crater soils and the global martian average. *Journal of*
517 *Geophysical Research: Planets*, *122*(12), 2623–2643.
- 518 Rampe, E., Blake, D., Bristow, T., Ming, D., Vaniman, D., Morris, R., . . . others
519 (2020). Mineralogy and geochemistry of sedimentary rocks and eolian sedi-
520 ments in Gale Crater, Mars: A review after six earth years of exploration with
521 Curiosity. *Geochemistry*, *80*(2), 125605.
- 522 Rapin, W., Ehlmann, B., Dromart, G., Schieber, J., Thomas, N., Fischer, W., . . .
523 others (2019). An interval of high salinity in ancient Gale Crater lake on Mars.
524 *Nature Geoscience*, *12*(11), 889–895.
- 525 Singer, R. B. (1985). Spectroscopic observation of Mars. *Advances in Space Re-*
526 *search*, *5*(8), 59–68.
- 527 Squyres, S. W., Arvidson, R. E., Ruff, S., Gellert, R., Morris, R., Ming, D., . . . oth-
528 ers (2008). Detection of silica-rich deposits on Mars. *Science*, *320*(5879),
529 1063–1067.
- 530 Sutter, B., Mcadam, A. C., Mahaffy, P. R., Ming, D. W., Edgett, K. S., Rampe,
531 E. B., . . . others (2017).
532 *Journal of Geophysical Research: Planets*, *122*(12), 2574–2609.
- 533 Tosca, N. J., McLennan, S. M., Clark, B. C., Grotzinger, J. P., Hurowitz, J. A.,
534 Knoll, A. H., . . . Squyres, S. W. (2005). Geochemical modeling of evaporation

- 535 processes on Mars: Insight from the sedimentary record at Meridiani Planum.
 536 *Earth and Planetary Science Letters*, 240(1), 122–148.
- 537 Tosca, N. J., McLennan, S. M., Lindsley, D. H., & Schoonen, M. A. (2004). Acid-
 538 sulfate weathering of synthetic martian basalt: The acid fog model revisited.
 539 *Journal of Geophysical Research: Planets*, 109(E5).
- 540 Treguier, E., d’Uston, C., Pinet, P. C., Berger, G., Toplis, M. J., McCoy, T. J., ...
 541 Brückner, J. (2008). Overview of Mars surface geochemical diversity through
 542 Alpha Particle X-Ray Spectrometer data multidimensional analysis: First at-
 543 tempt at modeling rock alteration. *Journal of Geophysical Research: Planets*,
 544 113(E12).
- 545 Vaniman, D. T., Bish, D. L., Chipera, S. J., Fialips, C. I., Carey, J. W., & Feldman,
 546 W. C. (2004). Magnesium sulphate salts and the history of water on Mars.
 547 *Nature*, 431(7009), 663–665.
- 548 Vaniman, D. T., & Chipera, S. J. (2006). Transformations of Mg-and Ca-sulfate hy-
 549 drates in Mars regolith. *American Mineralogist*, 91(10), 1628–1642.
- 550 Vaniman, D. T., Martínez, G. M., Rampe, E. B., Bristow, T. F., Blake, D. F., Yen,
 551 A. S., ... Sumner, D. Y. (2018). Gypsum, bassanite, and anhydrite at Gale
 552 Crater, Mars. *American Mineralogist*, 103(7), 1011–1020.
- 553 Wang, A., Haskin, L. A., Squyres, S. W., Jolliff, B. L., Crumpler, L., Gellert, R., ...
 554 others (2006). Sulfate deposition in subsurface regolith in Gusev Crater, Mars.
 555 *Journal of Geophysical Research: Planets*, 111(E2).
- 556 Wiens, R. C., Maurice, S., Barraclough, B., Saccoccio, M., Barkley, W. C., Bell,
 557 J. F., ... others (2012). The ChemCam instrument suite on the Mars Science
 558 Laboratory (MSL) rover: Body Unit and combined system tests. *Space science*
 559 *reviews*, 170(1-4), 167–227.
- 560 Wiens, R. C., Maurice, S., Lasue, J., Forni, O., Anderson, R., Clegg, S., ... others
 561 (2013). Pre-flight calibration and initial data processing for the ChemCam
 562 laser-induced breakdown spectroscopy instrument on the Mars Science Labora-
 563 tory rover. *Spectrochimica Acta Part B: Atomic Spectroscopy*, 82, 1–27.
- 564 Yen, A. S., Gellert, R., Schröder, C., Morris, R. V., Bell, J. F., Knudson, A. T., ...
 565 others (2005). An integrated view of the chemistry and mineralogy of martian
 566 soils. *Nature*, 436(7047), 49–54.
- 567 Yen, A. S., Morris, R., Clark, B. C., Gellert, R., Knudson, A., Squyres, S., ... oth-
 568 ers (2008). Hydrothermal processes at Gusev Crater: An evaluation of Paso
 569 Robles class soils. *Journal of Geophysical Research: Planets*, 113(E6).

Figure 1.

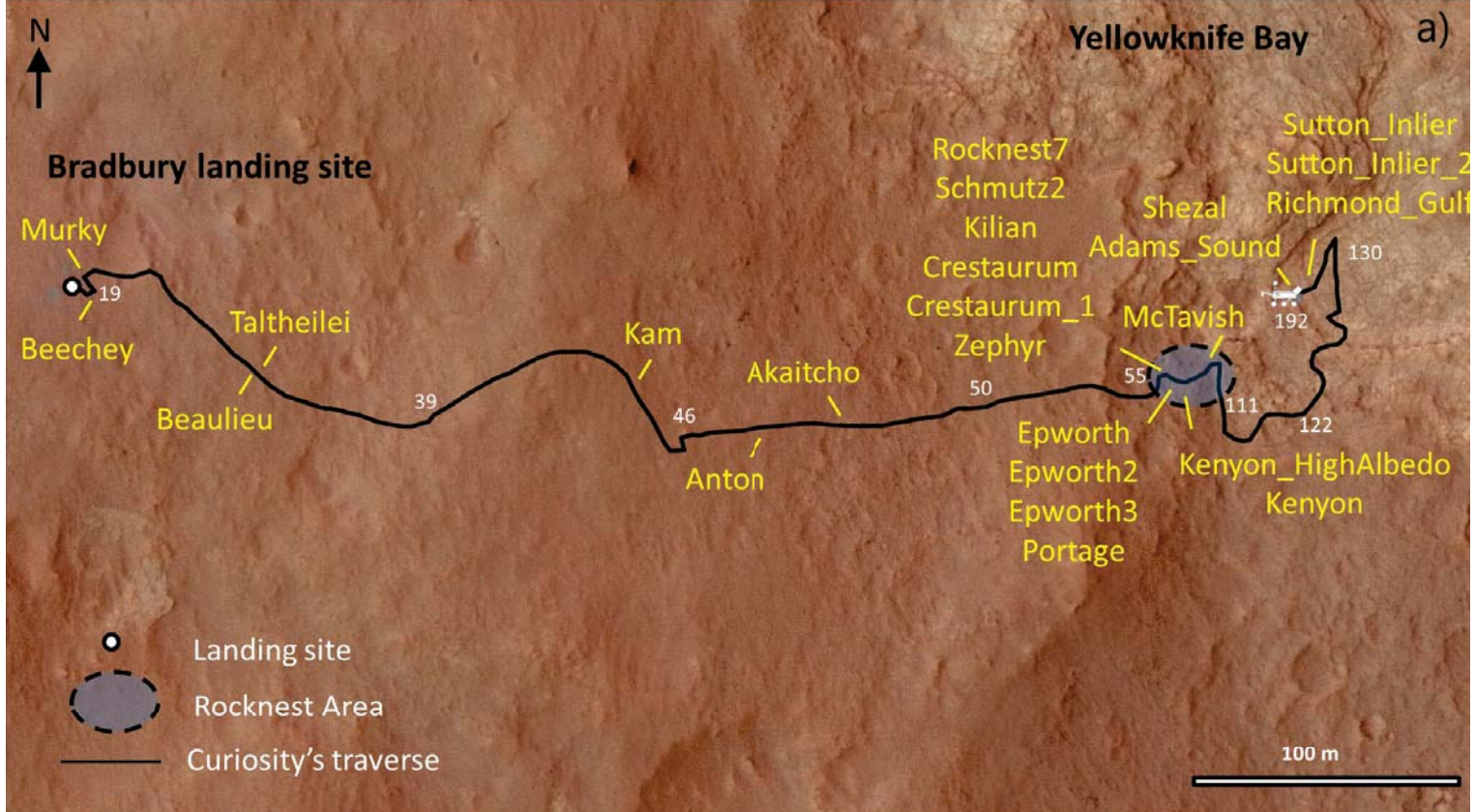


Figure 2.

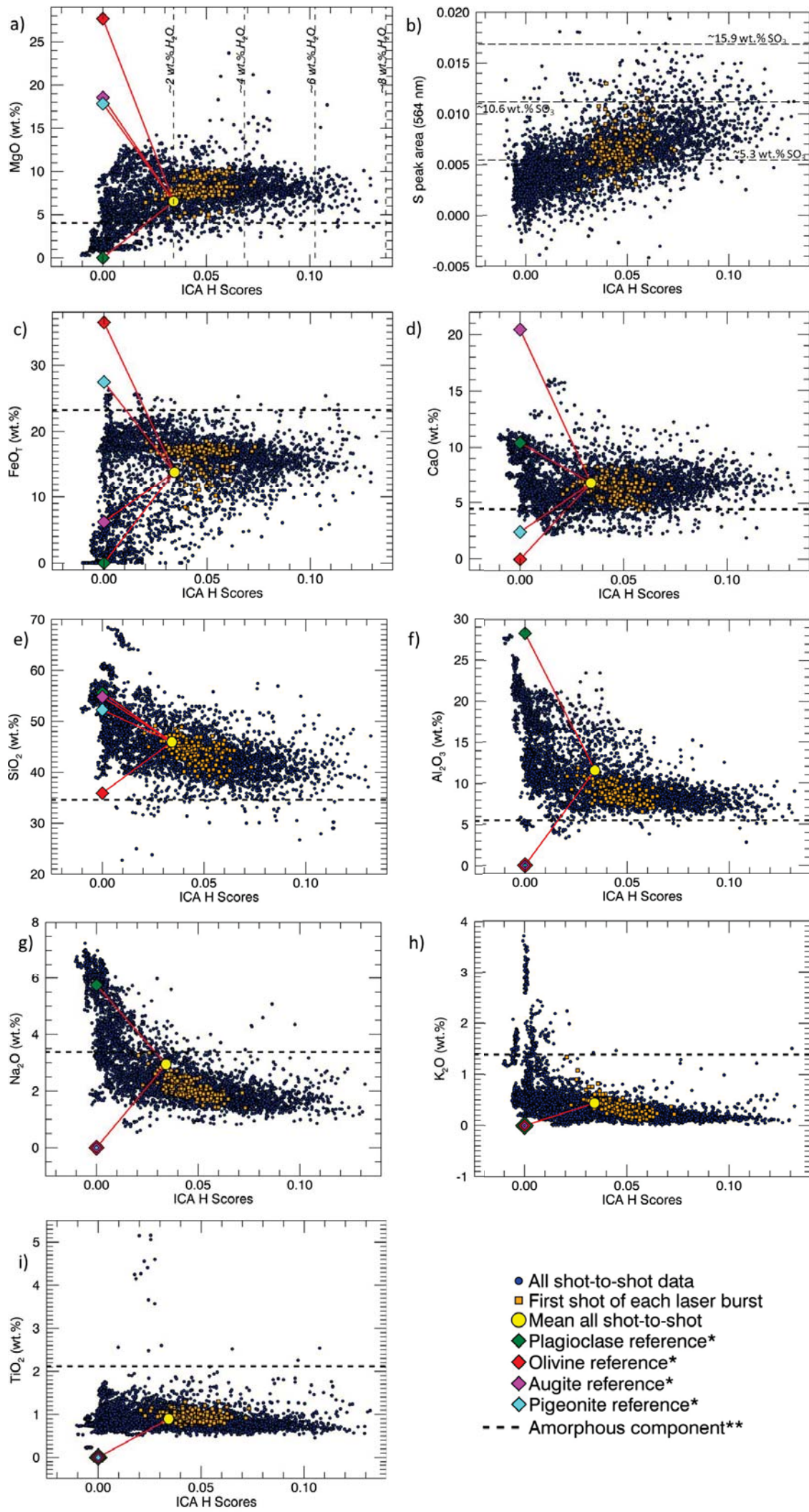


Figure 3.

